Title
Optimization criteria for coplanar-grid detectors

Author
Amman, M.

Publication Date
1999

LBNL-41702
Preprint

ERNEST ORLANDO LAWRENCE
BERKELEY NATIONAL LABORATORY

Optimization Criteria for Coplanar-Grid Detectors

M. Amman and P.N. Luke

Engineering Division

January 1999

Submitted to
IEEE Transactions
on Nuclear Science

DISCLAIMER

LBNL-41702

Optimization Criteria for Coplanar-Grid Detectors

M. Amman and P.N. Luke

Engineering Division
Ernest Orlando Lawrence Berkeley National Laboratory
University of California
Berkeley, California 94720

January 1999

This work was supported by the Department of Defense Office of Special Technology, Technical Support Working Group (TSWG), Project Number T-135, through the U.S. Department of Energy under Contract No. DE-AC03-76SF00098.

Optimization Criteria for Coplanar-Grid Detectors

M. Amman and P. N. Luke
Ernest Orlando Lawrence Berkeley National Laboratory
University of California, Berkeley, California 94720

Abstract

The coplanar-grid charge-sensing technique is a powerful method to achieve excellent spectroscopic performance with large-volume, CdZnTe-based, gamma-ray detectors despite the poor charge transport characteristics of the CdZnTe material. Critical to the success of the technique are the charge induction characteristics of the sensing-grid electrodes as governed by the detector geometry and the grid design. In this paper we demonstrate through numerical calculations of the detector response that the criteria for optimizing the grid design depend on the particular method in which the coplanar-grid technique is implemented. We present the fundamental design criteria in terms of the desired charge induction on the grid electrodes for the commonly used coplanar-grid implementations.

I. INTRODUCTION

The coplanar-grid charge-sensing technique has led to large-volume, CdZnTe-based, gamma-ray detectors with excellent energy resolution while operating at room temperature [1-4]. The technique accomplishes this by reducing or eliminating a number of the effects caused by the poor charge carrier transport of the CdZnTe material. However, in order to obtain the best possible energy resolution with the lowest amount of spectral background, care must be taken when designing the coplanar-grid electrode structure. In a previous publication, we demonstrated that the effectiveness of the coplanar-grid technique could be compromised by nonuniform charge induction characteristics across the detector, as governed by the detector geometry and grid design [5]. We concluded, based on modeling results and experimental measurements, that the charge induction on each of the two charge-sensing grid electrodes needed to be spatially uniform. More recently, however, He et al. [6] concluded that for optimal performance the charge induction on the two grid electrodes must be identical but not necessarily spatially uniform. These two seemingly different conclusions are both correct, and their difference is the result of a difference in the implementation of the coplanar-grid technique in the two studies.

A number of distinct implementations of the coplanar-grid technique presently exist [2,4,7]. Optimum detector performance is not necessarily achieved in the same manner for each of these variations. This distinction between the optimum charge induction characteristics for the various coplanar-grid implementations has not been made previously, yet understanding this distinction is crucial in designing coplanar-grid detectors to achieve the best possible energy resolution. This paper more fully elucidates the requirements for optimum coplanar-grid detector performance. We accomplish this through simple detector modeling. The implications of these requirements to practical grid designs are also given. We begin with a description of the coplanar-grid charge-sensing technique in the following section.

II. COPLANAR-GRID CHARGE SENSING

The basic structure and operation of a coplanar-grid detector are illustrated in Figure 1. The detector consists of a radiation-sensitive semiconductor crystal (such as CdZnTe) with a full-area electrical contact on one detector surface and on the opposing surface a contact segmented into strips that are interconnected to form two interdigitated coplanar grids. A large bias V_b is applied between the full contact and the grid electrodes so that the charge carriers created by radiation interactions within the detector crystal are collected across the detector. The bias polarity is such that the electrons drift towards the grid electrodes. A bias V_g is also applied between the two grid electrodes to ensure that these electrons are only collected on one of the grids, referred to as the collecting grid. This bias is small relative to V_b so that the field within the bulk of the detector remains substantially uniform.

There are a number of variations of the coplanar-grid charge-sensing technique, yet the excellent gamma-ray detection performance achieved with each implementation results from the same two separate aspects of the technique. The first is that the majority of the charge induction occurs when charge carriers drift through a small volume of the detector near the coplanar-grid electrodes. To see how this is accomplished and why it is important, consider a charge - Q drifting from the full-area electrode in a straight trajectory to one of the collecting grid strips, as illustrated in Figure 1a. The induced charge signals from the detector electrodes as a result of this drifting charge can be determined using the weighting potential method, which has been discussed in detail elsewhere [7-9]. The result of such a calculation for the induced signals from the two grid electrodes assuming no charge trapping is shown in Figure 1b. For this grid design, the two signals are the same until the charge drifts near the grids, at which point the signal from the collecting grid (*cg*) rapidly increases to - Q while that from the other noncollecting grid (*ncg*) decreases to zero. This behavior can be understood based on the idea that the charge induced on an electrode is proportional to the number of electrostatic field flux lines connecting the drifting charge to the particular electrode. For the case when - Q is far from the grids, the flux lines will be evenly distributed between the two grids because of their interdigitated pattern and their identical size. As the charge moves towards the grids, the density of the flux lines terminating on the grids increases yet remains equally shared between the two grids. However, when the charge drifts into the region very near the grids, it becomes much closer to the particular collecting grid strip on which collection will ultimately take place relative to the distance to the other grid strips. The number of flux lines terminating on this collecting

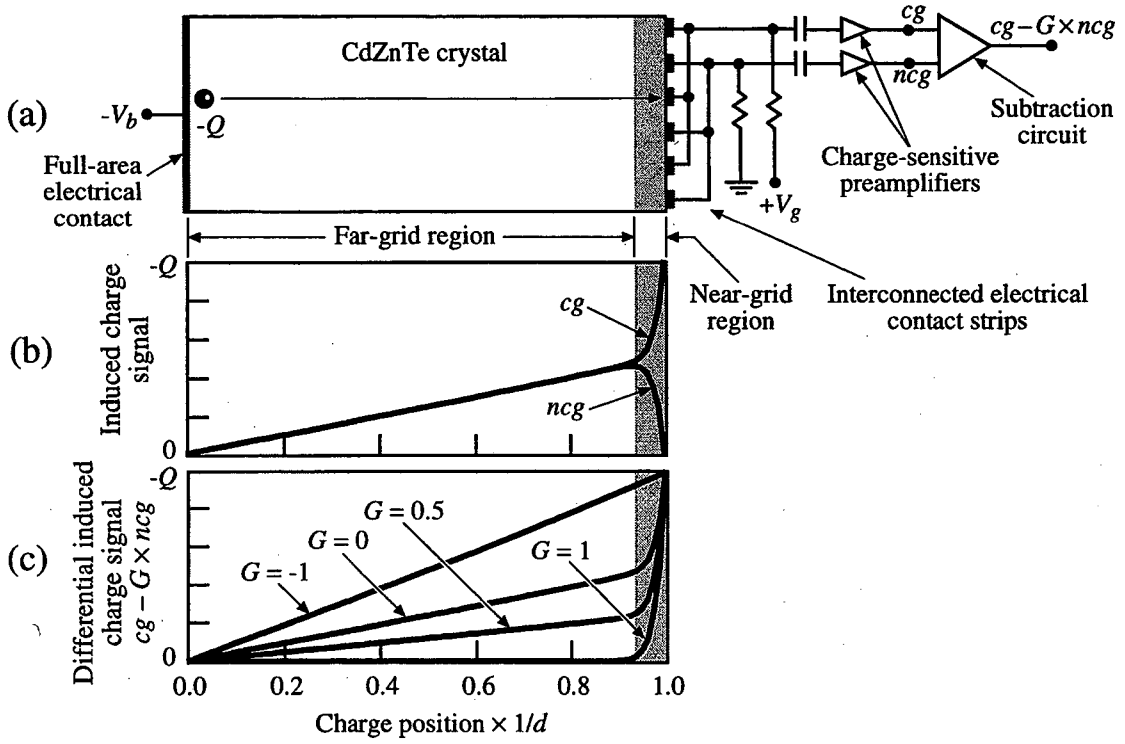

Figure 1. **(a)** Schematic drawing of a conventional coplanar-grid detector. **(b)** Calculated induced charge signals from the collecting grid (*cg*) and noncollecting grid (*ncg*) of a coplanar-grid detector as a function of the position of a drifting charge - *Q* originating near the full-area cathode and ultimately collected by the collecting grid as illustrated in (a). The charge position has been normalized by the detector thickness *d*. The detector was assumed to be 10 mm thick and infinite in size in the lateral dimensions, and the strip width of the grid electrodes was 0.25 mm with a gap spacing of 0.25 mm. Charge trapping was not included in the calculation. The region of the detector in which the drifting charge produces the greatest change in the induced charge signals is defined as the near-grid region (shaded region), whereas the remainder of the detector volume is referred to as the far-grid region. **(c)** Difference between the collecting- and noncollecting-grid signals for various values of the relative gain *G*.

grid strip will then rapidly increase at the expense of all other grid strips, thus producing the rapid rise in collecting grid signal and the corresponding fall in noncollecting grid signal. We refer to this part of the detector where there is a rapid change in the induced charge signals as the *near-grid region* and the remainder of the detector as the *far-grid region.*

If the detector signal is formed by the direct subtraction of the noncollecting grid signal from that of the collecting grid (relative gain $G = 1$ in Figure 1c), a non-zero detector signal results only when the charge carriers move into the near-grid region. When a gamma-ray interacts within the far-grid region of this detector, the collection of the generated electrons through the near-grid region produces a detector signal that is proportional only to the number of electrons being collected through the near-region and is therefore unaffected by the hole transport. This, in principle, eliminates the problem of poor hole collection found in materials such as CdZnTe.

The second aspect of the coplanar-grid technique that leads to improved spectroscopic performance is that it provides a means to correct for electron trapping. To illustrate the problem introduced by electron trapping, consider three separate gamma-ray interaction events occurring at different distances from the grid electrodes of the detector described in Figure 1. The calculated detector pulses resulting from these events are shown superimposed in Figure 2a. Here the detector signal is the direct subtraction of the two grid signals, and an amount of electron trapping typical of that of CdZnTe has been assumed. For the event that occurs a small distance from the grid electrodes ($z_o = 2$ mm), nearly a full energy pulse height (- *Q*) is produced since little electron trapping takes place during the short electron drift to the near-grid region. In contrast, the event near the full-area cathode ($z_o = 10$ mm) produces electrons that must drift nearly the entire depth of the detector before reaching the near-grid region and producing a net detector signal. Electron trapping occurs during this transit, leading to a significant pulse height deficit (approximately 20 %). This pulse-height variation with depth left uncorrected would substantially degrade the energy resolution of the detector.

Two general methods have been introduced to correct for the electron-trapping problem in the coplanar-grid charge-sensing technique: *charge induction optimization* and *depth-sensing based correction.* In the charge induction optimization method, a specific amount of charge induction is introduced for carriers drifting within the far-grid region in order to make up for the electron loss during the transit through this region. One way to accomplish this is by adjusting the relative gain (*G*) of the two grid signals prior to subtraction. We refer to this implementation of the coplanar-grid technique as the *conventional* or *differential-gain* method [2]. By reducing *G* from 1, charge induction is introduced in the subtracted detector signal for carriers drifting through the

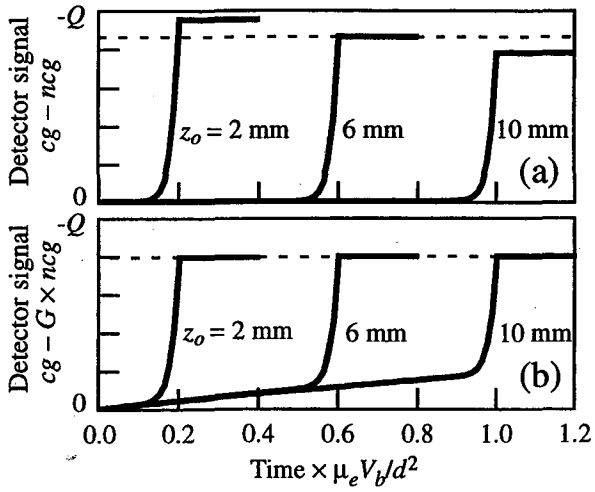

Figure 2. Calculated detector pulses resulting from three gamma-ray interaction events taking place at different depths within the coplanar-grid detector described in Figure 1. The pulses are plotted as a function of the normalized time and superimposed so that zero time corresponds to the interaction event. The depths (z_o) of the interaction events from the grid electrode surface are 2 mm, 6 mm, and 10 mm. The pulses were calculated assuming a detector thickness $d = 10$ mm, a bias $V_b = 1000$ V, and an electron mobility-lifetime product $\mu_e\tau_e = 4\times10^{-3}$ cm²/V. The typically small contribution to the signals from hole collection was neglected. **(a)** Detector pulses formed from the direct subtraction of the noncollecting grid signal from the collecting grid signal. **(b)** Detector pulses formed when the differential gain between the two grid signals prior to subtraction was optimized in order to minimize the pulse height variation with depth of interaction caused by electron trapping. The optimum differential gain for this detector and operating conditions is $G = 0.58$.

far-grid region (see Figure 1c). By optimizing G, near-perfect compensation can be made for the electron loss during the drift through the far-grid region. This is demonstrated in Figure 2b where, as in Figure 2a, we have plotted the calculated detector pulses from gamma-ray interaction events taking place at different depths within the detector. The detector signals in this case were formed by subtracting an optimum fraction ($G = 0.58$) of *ncg* from *cg* and show little pulse-height variation with depth.

Another charge induction optimization method is illustrated in Figure 3. This is the *single-electrode-readout* implementation of the coplanar-grid technique [7]. In this method, the detector signal is read out from only the collecting grid thereby reducing electronic noise and allowing the use of simple, single-amplifier detection electronics. Optimization of the charge induction in the far-grid region is made in this case by adjusting the relative areas of the two grid electrodes. This is shown in Figure 3b where we have plotted the induced charge signal on the collecting grid for various ratios of the collecting-grid strip width (w_c) to the noncollecting-grid strip width (w_{nc}). Notice that as the w_c/w_{nc} ratio is reduced, the charge induction in the far-grid region decreases. This results from the screening effect of the noncollecting grid. As w_c/w_{nc} decreases, fewer electrostatic field flux lines from the drifting charge will terminate on the collecting grid since it simply occupies a smaller area of the detector surface, while that on the noncollecting grid will increase. Fewer flux lines means a smaller amount of induced charge. The adjustment of the relative grid areas can therefore be used to match the amount of charge induction in the far-grid region to the level of electron trapping that exists in the

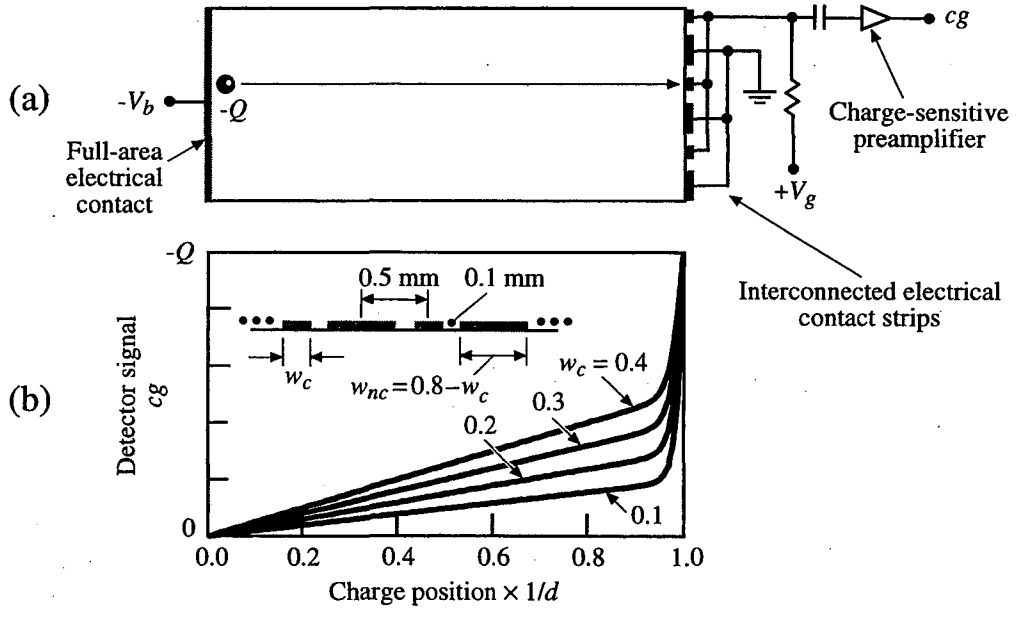

Figure 3. (a) Schematic drawing of a single-electrode-readout coplanar-grid detector. **(b)** Calculated induced charge signal from the collecting grid (*cg*) of a single-electrode-readout coplanar-grid detector as a function of the position of a drifting charge - Q originating near the full-area cathode and ultimately collected by the collecting grid as illustrated in (a). The detector was assumed to be 10 mm thick and infinite in size in the lateral dimensions. Charge trapping was not included in the calculation. The induced charge signal is shown for a number of different collecting grid strip widths, w_c. As w_c was varied, so was the noncollecting grid strip width w_{nc} in order to maintain a constant center-to-center electrode spacing of 0.5 mm and a constant gap spacing of 0.1 mm.

detector material. In practice the grid electrodes are designed assuming a specific electron mobility-lifetime product and a desired operating detector bias. Once fabricated, fine optimization of the detector performance is accomplished by adjusting the detector bias, which in effect adjusts the amount of electron trapping.

The other general method of electron-trapping correction is the depth-sensing based correction [3, 4]. In this method the detector signal is formed from the directly subtracted grid signals ($G = 1$). Electron trapping compensation is realized separately by measuring the depth of the gamma-ray interaction within the detector and subsequently applying a correction to the measured detector signal based on the interaction depth. The detector structure is similar to that of the differential-gain method shown in Figure 1a, except that an additional charge-sensitive preamplifier is used in order to measure the induced charge signal on the full-area cathode. For CdZnTe-based detectors, the hole transport is very poor. This leads to a cathode signal pulse height that is approximately proportional to $E_\gamma z_o$, where E_γ is the energy of the gamma-ray and z_o is the depth of the gamma-ray interaction measured from the grid electrode surface. The pulse height measured from the subtracted grid signals ($cg - ncg$) is approximately proportional to E_γ. Therefore, by taking the ratio of the cathode pulse height to the subtracted grid signal pulse height, the depth of the gamma-ray interaction is obtained for events in the far-grid region. Though requiring more complex electronics than the other coplanar-grid implementations, this method allows for a pulse height deficit correction that is an arbitrary function of the measured depth.

III. Theoretical Methods

Each of the three implementations of the coplanar-grid charge-sensing technique described in the previous section can be used to produce large-volume, CdZnTe-based, gamma-ray detectors with excellent energy resolution. However, to accomplish this, the charge carrier transport of the material must be uniform [10], and the detector response must be uniform for events taking place at different locations across the detector. Here we will consider only the issue of detector response uniformity and assume that the charge transport is perfectly uniform.

In the previous section, the issue of uniformity of the detector response with the depth of gamma-ray interaction (z_o) was addressed. Just as important is the uniformity of the detector response with the lateral location of the interaction event (x_o, y_o). This uniformity is dictated by the detector geometry and the grid design. In order to demonstrate the effect of grid design on detector response uniformity, we have calculated the induced charge signals resultant from gamma-ray interaction events at various locations throughout the detector volume using a simple detector model.

There are a number of approximations made in our detector model, yet the model still retains the essential physics of the system. First, we have neglected hole transport. This is justified since state-of-the-art high-pressure Bridgman grown CdZnTe material has an electron mobility-lifetime product that is about two orders of magnitude greater than that of the holes [11]. Second, straight trajectories into the collecting grid electrodes were assumed. We chose to look at events that originate directly beneath collecting-grid strips. Therefore, the deviation of the actual trajectory from this straight-line trajectory is minimal. Third, a constant electric field leading to a constant electron drift velocity was assumed throughout the detector volume. Finally, when electron trapping was included in the calculations, a single electron lifetime was used without any detrapping of the electrons.

Using these approximations, the induced charge signals were determined using the weighting potential method [7-9]. A detector size of approximately 1 cm^3 was used for all the calculations. For the calculations that included electron trapping effects, an electron mobility-lifetime product of 4×10^{-3} cm^2/V and a detector bias of 1000 V were assumed. The results for a number of different grid designs are presented and discussed in the next section.

IV. Optimum Coplanar-Grid Design

The problem of poor charge induction uniformity and its relation to the grid electrode design are illustrated in Figures 4-6. Here we consider the simple coplanar-grid detector design shown in Figure 4. The grid electrode structure of this design is composed of a series of linear strip electrodes of equal width and spacing. The design begins with a collecting grid strip at the top of the grid electrode surface and ends with a noncollecting grid strip at the bottom. This simple termination of the grid electrode pattern is the origin of the uniformity problem. This can be seen in Figure 5 where we have plotted the induced charge signals from the two grids as a result of a charge - Q drifting from the full-area cathode to the grid anodes. The signals are shown for three different lateral points of origin (x_o) of the drifting charge. The charge induction is similar for the three cases when - Q drifts through the near-grid region because of the ultimate collection at a collecting grid strip. However, the induction within the far-grid region is quite different between the three cases. For the case when the charge is drifting through the top part of the detector ($x_o = x_t$), the charge induction is greater from the collecting grid. This occurs because at the top edge of the grid electrode structure is a collecting grid strip. The collecting grid is then as a whole closer to the top of the detector than is the noncollecting grid. The closer proximity of the collecting grid to the drifting charge produces a greater charge induction on the collecting grid. The opposite is then true of the $x_o = x_b$ case in which the noncollecting grid dominates, leading to greater charge induction on the noncollecting grid when - Q drifts through the far-grid region. Finally, the $x_o = x_m$ case produces identical charge induction on the two grids.

The impact of this poor charge induction uniformity on the detector response is shown in Figure 6. In this figure, the calculated detector pulses resulting from gamma-ray interaction events at various depths and lateral locations within the detector have been plotted. In the calculation of the detector signals, electron trapping was not included, yet there is a substantial pulse height variation with the depth of the gamma-ray interaction that is evident near the top and bottom of the detector. This pulse height variation also depends on the lateral location of the interaction event, and therefore the simple charge trapping correction schemes discussed previously will not be effective in reducing the pulse height

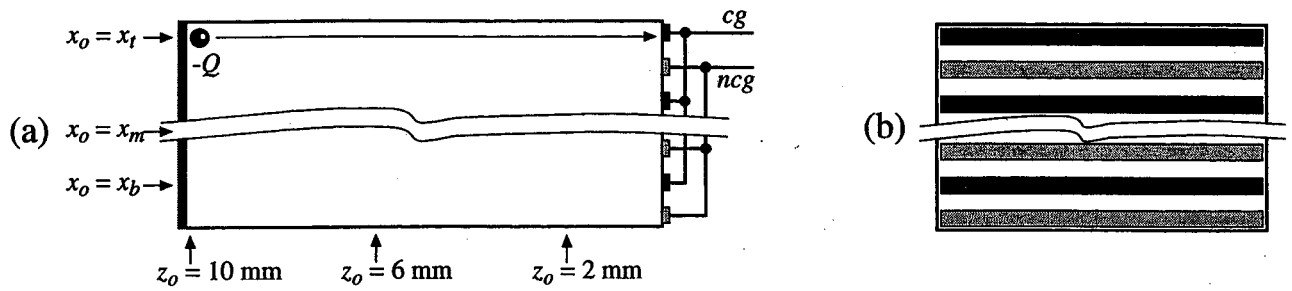

Figure 4. Schematic drawing of a coplanar-grid detector with a simple grid design. The grid electrode surface has an area of 9 mm × 9 mm, and the detector thickness is 10 mm. There are 18 grid strips of 0.25 mm width and 0.25 mm spacing in this design. **(a)** Side view of the detector showing the interaction locations (x_o, z_o) assumed in the calculations. **(b)** View of the grid electrode surface.

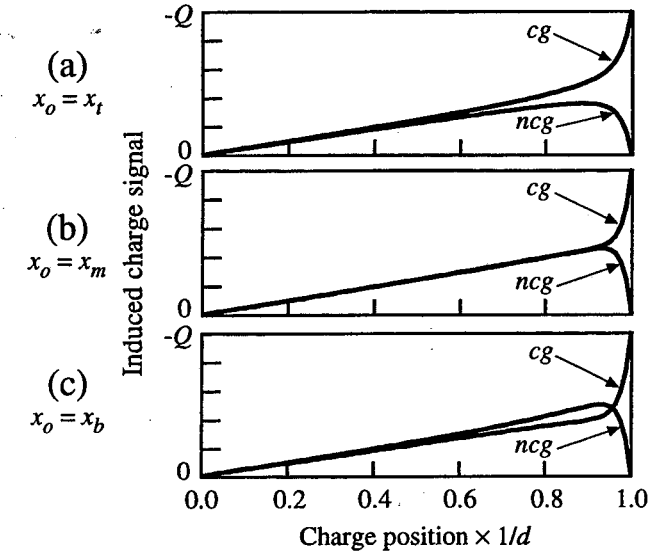

Figure 5. Calculated induced charge signals from the grid electrodes of the coplanar-grid detector described in Figure 4 as a function of the position of a drifting charge - Q originating near the full-area cathode (z_o = 10 mm) and ultimately collected by a collecting grid strip. Charge trapping was not included in the calculation. **(a)** Event near the top of the detector at $x_o = x_t$. **(b)** Event near the middle of the detector at $x_o = x_m$. **(c)** Event near the bottom of the detector at $x_o = x_b$.

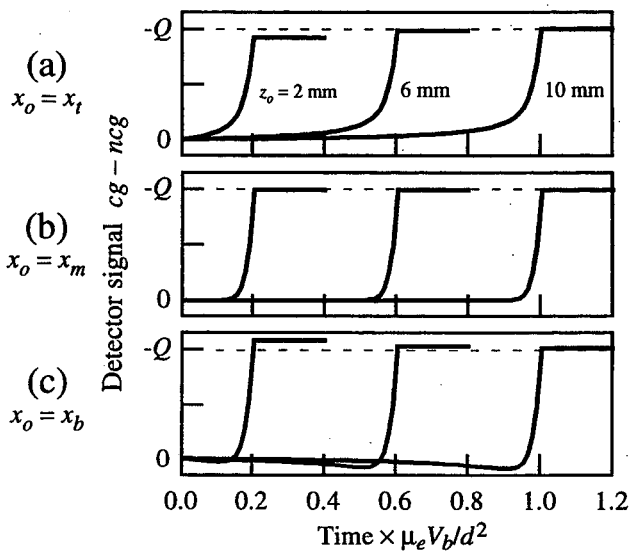

Figure 6. Calculated detector pulses resulting from three gamma-ray interaction events taking place at different depths within the coplanar-grid detector described in Figure 4. The depths of the interaction events from the grid electrode surface are 2 mm, 6 mm, and 10 mm. Charge trapping was not included in the calculation. **(a)** Events near the top of the detector at $x_o = x_t$. **(b)** Events near the middle of the detector at $x_o = x_m$. **(c)** Events near the bottom of the detector at $x_o = x_b$.

variation. Consequently, a degradation of the energy resolution of the detector will result.

One solution to this problem is to design the grid electrodes so that the detector signal is uniform with the lateral location of the interaction event. However, each of the previously described coplanar-grid implementations derives the detector signal from the individual grid signals in a different manner. This difference then leads to a difference in the grid design requirements for optimum gamma-ray detection performance. Consider first the differential-gain coplanar-grid implementation. The detector signal for this scheme is $cg - G \times ncg$. The differential gain G is a parameter that depends on the electron trapping level in the detector and is not precisely known at the detector design stage. Consequently, the uniformity of the detector signal can only be ensured if the individual grid signals are separately made uniform. Therefore the grid electrodes must be designed so that the charge induction on each grid does not vary with the lateral location of the drifting charge. Similar to this is the grid design requirement of the single-electrode-readout implementation. Here the detector signal is cg. The desired grid design is then one that produces a collecting grid charge induction that does not vary with the lateral location of the drifting charge. The depth-sensing implementation, however, has a slightly less restrictive grid design requirement than the other two implementations. The detector signal of the depth-sensing scheme is the direct subtraction of the two grid signals, $cg - ncg$. As with the differential-gain implementation, uniformity in this detector signal can be achieved by requiring that the charge induction on the grids be separately uniform. However, uniformity can also be achieved by making the charge induction within the far-grid region on the collecting grid equal to that on the noncollecting grid. The charge induction on each grid, therefore, does not necessarily need to be spatially uniform. The identical charge induction of the two grids then leads to a uniform detector

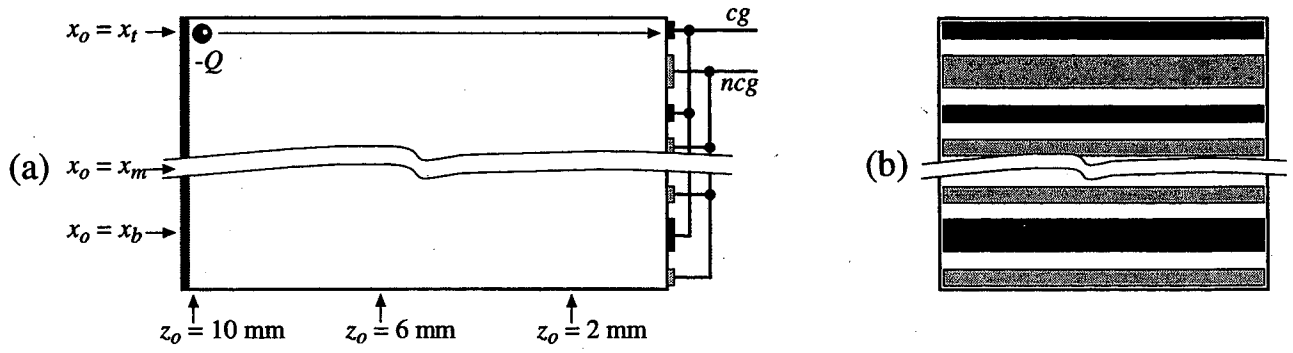

Figure 7. Schematic drawing of a coplanar-grid detector with an edge corrected grid design. The grid electrode surface has an area of 9.5 mm × 9.5 mm, and the detector thickness is 10 mm. The interior portion of this grid pattern is similar to that of Figure 4 in that the strips are 0.25 mm wide and spaced by 0.25 mm. In this design, however, the strip next to the edge grid strip on each side of the detector has been made wider in order to correct for an edge effect. **(a)** Side view of the detector showing the interaction locations (x_o, z_o) assumed in the calculations. **(b)** View of the grid electrode surface.

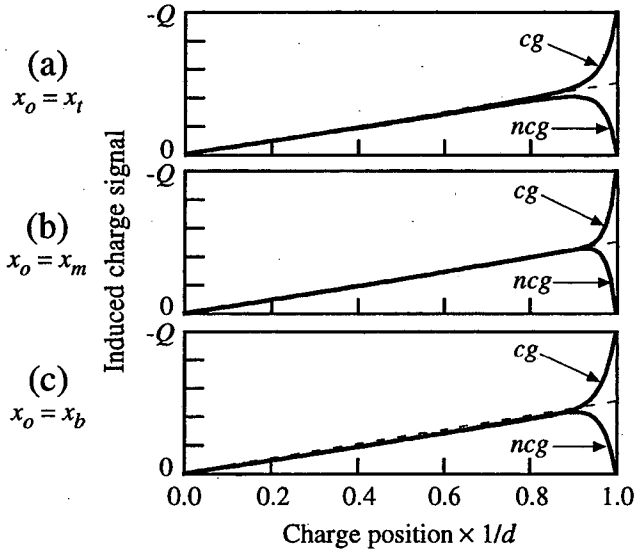

Figure 8. Calculated induced charge signals from the grid electrodes of the coplanar-grid detector described in Figure 7 as a function of the position of a drifting charge - Q originating near the full-area cathode (z_o = 10 mm) and ultimately collected by a collecting grid strip. Charge trapping was not included in the calculation. **(a)** Event near the top of the detector at $x_o = x_t$. **(b)** Event near the middle of the detector at $x_o = x_m$. **(c)** Event near the bottom of the detector at $x_o = x_b$.

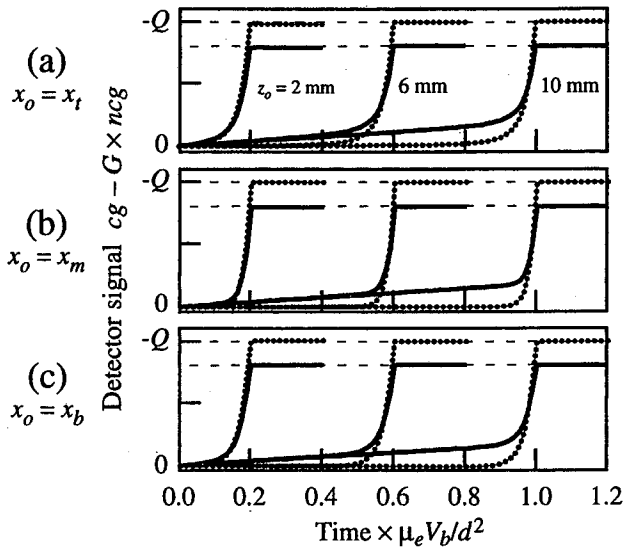

Figure 9. Calculated detector pulses resulting from three gamma-ray interaction events taking place at different depths within the coplanar-grid detector described in Figure 7. The depths of the interaction events from the grid electrode surface are 2 mm, 6 mm, and 10 mm. The pulses plotted with dotted lines were calculated assuming no trapping and $G = 1$. Those plotted with solid lines were calculated assuming the presence of trapping and an optimum differential gain which was determined to be $G = 0.58$. **(a)** Events near the top of the detector at $x_o = x_t$. **(b)** Events near the middle of the detector at $x_o = x_m$. **(c)** Events near the bottom of the detector at $x_o = x_b$.

signal of zero within the far-grid region. Within the near-grid region a net detector signal will be developed that is proportional to the number of electrons drifting through the region and be substantially independent of the lateral location of the drifting charge.

The practical use of the above optimum grid design criteria will now be demonstrated through two examples. Consider first the detector design of Figure 7. The grid pattern in this example is the same as the simple one of Figure 4, except that the grid strips nearest to the two edge grid strips have been widened. This compensates for the dominating effect of the edge grid strips, thereby producing more laterally uniform charge induction characteristics on each grid. The improved characteristics are shown in the induced charge plots of Figure 8. Relative to the plots of Figure 5, these characteristics are much more uniform in that the induced charge signals from the grids change very little in the far-grid region as the interaction location is changed from the top of the detector ($x_o = x_t$) to the bottom of the detector ($x_o = x_b$). This leads to the improved detector response shown in Figure 9. In this figure, the calculated detector pulses resulting from gamma-ray interactions throughout the detector volume are plotted. The pulses plotted with dotted lines do not include electron trapping effects and are formed by the direct subtraction of the two grid signals ($G = 1$). These

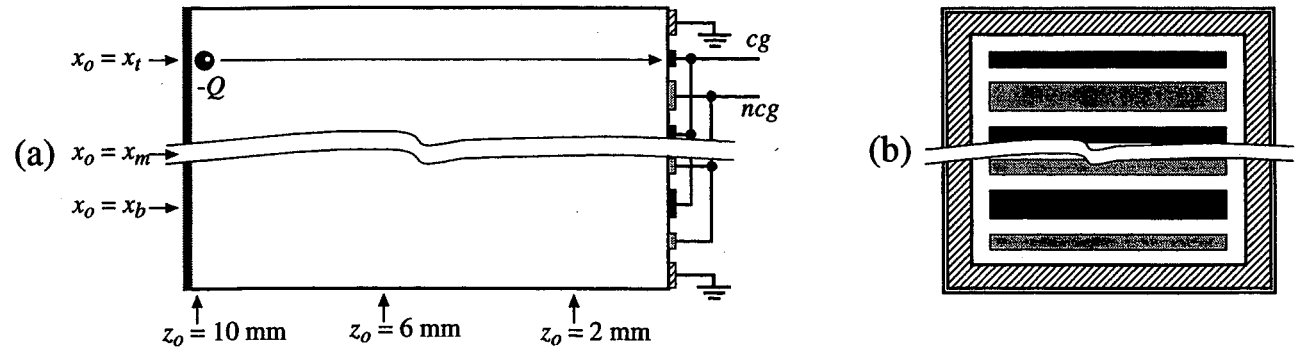

Figure 10. Schematic drawing of a coplanar-grid detector with an edge-corrected guard-ring grid design. The grid electrode surface has an area of 10 mm × 10 mm, and the detector thickness is 10 mm. The interior portion of this grid pattern is similar to that of Figure 4 in that the strips are 0.25 mm wide and spaced by 0.25 mm. This design, however, has a guard-ring electrode surrounding the grid electrodes, and the grid strip next to the edge grid strip on each side of the detector has been made wider in order to correct for an edge effect. **(a)** Side view of the detector showing the interaction locations (x_o, z_o) assumed in the calculations. **(b)** View of the grid electrode surface.

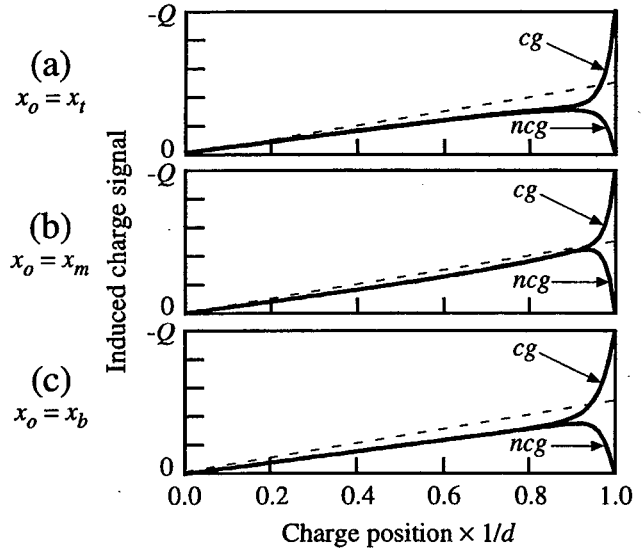

Figure 11. Calculated induced charge signals from the grid electrodes of the coplanar-grid detector described in Figure 10 as a function of the position of a drifting charge - Q originating near the full-area cathode (z_o = 10 mm) and ultimately collected by a collecting grid strip. Charge trapping was not included in the calculation. **(a)** Event near the top of the detector at $x_o = x_t$. **(b)** Event near the middle of the detector at $x_o = x_m$. **(c)** Event near the bottom of the detector at $x_o = x_b$.

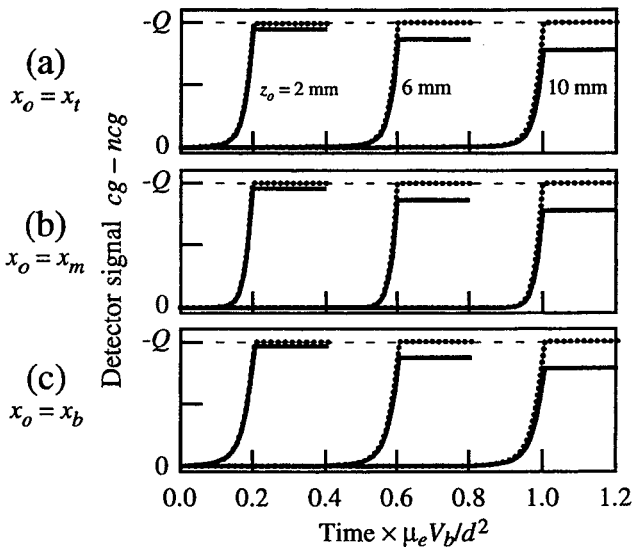

Figure 12. Calculated detector pulses resulting from three gamma-ray interaction events taking place at different depths within the coplanar-grid detector described in Figure 10. The depths of the interaction events from the grid electrode surface are 2 mm, 6 mm, and 10 mm. The pulses plotted with dotted lines were calculated assuming no trapping while those plotted with solid lines include trapping effects. **(a)** Events near the top of the detector at $x_o = x_t$. **(b)** Events near the middle of the detector at $x_o = x_m$. **(c)** Events near the bottom of the detector at $x_o = x_b$.

pulses all have nearly the same pulse height independent of the interaction location. The edge effect problem detailed in Figures 4-6 has therefore been nearly eliminated by the simple change in the grid design. When electron trapping is taken into account, the pulse heights will exhibit a dependence on the depth of interaction. Since this is only a depth dependence, the differential-gain method or the depth-sensing method can be used to effectively correct for the pulse height variation. This is demonstrated in Figure 9 with the pulses plotted with solid lines. These pulses were calculated assuming electron trapping was present and that an optimal fraction of *ncg* was subtracted from *cg* in order to form the detector signal (differential-gain technique with $G = 0.58$). The resultant pulse heights vary little with the interaction location, thereby producing a detector with a good gamma-ray response.

The second detector design example highlights the difference between the grid design criterion of the differential-gain implementation and that of the depth-sensing implementation. The design, shown in Figure 10, is similar to that of Figure 7 except that a grounded guard ring has been placed at the perimeter of the grid electrode structure. The width of the guard ring and the grid strips nearest to the two

edge grid strips have been adjusted so that *cg* is nearly identical to *ncg* in the far-grid region (Figure 11). These charge induction characteristics should then produce near-optimal detector performance in the depth-sensing implementation. The detector response to gamma rays interacting at various locations within the detector volume is shown in Figure 12. The pulses plotted with dotted lines were calculated assuming no electron trapping. The detector response is uniform in this case since the pulse height is nearly independent of the interaction location. With the addition of electron trapping (pulses plotted with solid lines), a depth of interaction dependence is introduced into the pulse height. This pulse height variation can readily be corrected for through a depth measurement and subsequent pulse height adjustment. The depth-sensing method will therefore produce an excellent gamma-ray detection performance with this detector design.

In contrast, the differential-gain implementation will not produce optimal performance with this guard-ring detector design. From Figure 11 it is evident that the charge induction characteristics of the grids are not spatially uniform. The slope of the induced charge signals in the far-grid region is less near the edges of the detector than near the middle of the detector. This is a direct result of the presence of the guard ring. By adding the guard ring, some of the electrostatic field flux lines that would have terminated on the grid electrodes now terminate on the guard ring. This effect is stronger near the edges of the detector because of the closer proximity of the guard ring to the drifting charge. The decreased flux line density on the grids leads to decreased charge induction. This lack of uniformity of the charge induction in the far-grid region is a problem for the differential-gain implementation. In order to correct for electron trapping, this technique relies on introducing a specific amount of charge induction in the far-grid region by subtracting only a fraction G of *ncg* from *cg* in order to form the detector signal. Unfortunately, if *cg* and *ncg* vary laterally across the detector, as is the case here, then so will the optimal value of G. For example, the optimal level of G at $x_o = x_t$ is 0.46, whereas at $x_o = x_m$ it is 0.52. Since only one value of G can be set, there will be regions in the detector where the charge induction is less than optimum, thus resulting in a less than optimal gamma-ray detection performance.

V. SUMMARY

We have described simple design criteria, in terms of the grid charge induction characteristics, that need to be met in order to achieve the best possible gamma-ray detection performance with the coplanar-grid charge-sensing technique. We have demonstrated that the optimal charge induction characteristics depend on the method in which the coplanar-grid technique is implemented. For the differential-gain implementation, the charge induction on each grid due to charges drifting in the far-grid region should not vary across the detector. Otherwise, detector energy resolution is degraded. An optimum grid design is then one that produces spatially uniform charge induction characteristics on both grid electrodes. Likewise, the single-electrode-readout implementation requires spatially uniform charge induction on the collecting grid electrode. In contrast, the depth-sensing implementation does not necessarily require spatial uniformity of the grid charge induction for optimal detector performance. With this technique, optimal performance can be obtained by making the charge induction characteristics within the far-grid region of the collecting grid equal to that of the noncollecting grid. One implication of this is that a grid design containing a perimeter guard ring can produce optimal detector performance with the depth-sensing implementation, but the same design will produce less than optimal results with the differential-gain method.

VI. ACKNOWLEDGMENTS

This work was supported by the DOD Office of Special Technology, Technical Support Working Group (TSWG), Project Number T-135.

VII. REFERENCES

[1] P. N. Luke, "Single-polarity charge sensing in ionization detectors using coplanar electrodes," *Appl. Phys. Lett.*, vol. 65, pp. 2884-2886, 1994.

[2] P. N. Luke and E. E. Eissler, "Performance of CdZnTe coplanar-grid gamma-ray detectors," *IEEE Trans. Nucl. Sci.*, vol. 43, pp. 1481-1486, 1996.

[3] Z. He, G. F. Knoll, D. K. Wehe et al., "1-d position sensitive single carrier semiconductor detectors," *Nucl. Instrum. Methods A*, vol. 380, pp. 228-231, 1996.

[4] Z. He, G. F. Knoll, D. K. Wehe, and J. Miyamoto, "Position-sensitive single carrier CdZnTe detectors," *Nucl. Instrum. Methods A*, vol. 388, pp. 180-185, 1997.

[5] P. N. Luke, M. Amman, T. H. Prettyman, P. A. Russo, and D. A. Close, "Electrode design for coplanar-grid detectors," *IEEE Trans. Nucl. Sci.*, vol. 44, pp. 713-720, 1997.

[6] Z. He, G. F. Knoll, D. K. Wehe, and Y. F. Du, "Coplanar grid patterns and their effect on energy resolution of CdZnTe detectors," *Nucl. Instrum. Methods A*, vol. 411, pp. 107-113, 1998.

[7] M. Amman and P. N. Luke, "Coplanar-grid detector with single-electrode readout," *Proceedings of SPIE*, vol. 3115, pp. 205-213, 1997.

[8] W. Shockley, "Currents to conductors induced by a moving point charge," *J. Appl. Phys.*, vol. 9, pp. 635-636, 1938.

[9] S. Ramo, "Currents induced by electron motion," *Proc. I. R. E.*, vol. 27, pp. 584-585, 1939.

[10] M. Amman, J. S. Lee, and P. N. Luke, "Electron transport uniformity characterization of CdZnTe using alpha particles," *Proceedings of SPIE*, vol. 3446, pp. 179-190, 1998.

[11] C. Szeles and M. C. Driver, "Growth and properties of semi-insulating CdZnTe for radiation detector applications," *Proceedings of SPIE*, vol. 3446, pp. 2-9, 1998.

Ernest Orlando Lawrence Berkeley National Laboratory
One Cyclotron Road | Berkeley, California 94720

Prepared for the U.S. Department of Energy under Contract No. DE-AC03-76SF00098